



CHORUS

This is the accepted manuscript made available via CHORUS. The article has been published as:

Sensing with Exceptional Surfaces in Order to Combine Sensitivity with Robustness

Q. Zhong, J. Ren, M. Khajavikhan, D. N. Christodoulides, Ş. K. Özdemir, and R. El-Ganainy

Phys. Rev. Lett. **122**, 153902 — Published 16 April 2019

DOI: [10.1103/PhysRevLett.122.153902](https://doi.org/10.1103/PhysRevLett.122.153902)

Sensing with exceptional surfaces in order to combine sensitivity with robustness

Q. Zhong,¹ J. Ren,² M. Khajavikhan,² D.N. Christodoulides,² Ş.K. Özdemir,^{3,4} and R. El-Ganainy^{1,5,*}

¹*Department of Physics and Henes Center for Quantum Phenomena,
Michigan Technological University, Houghton, Michigan, 49931, USA*

²*College of Optics & Photonics-CREOL, University of Central Florida, Orlando, Florida, 32816, USA*

³*Department of Engineering Science and Mechanics,
The Pennsylvania State University, University Park, Pennsylvania 16802, USA*

⁴*Materials Research Institute, The Pennsylvania State University, University Park, PA 16802-6812, USA*

⁵*Department of Electrical and Computer Engineering,
Michigan Technological University, Houghton, Michigan, 49931, USA*

Exceptional points (EPs) are singularities that arise in non-Hermitian physics. Current research efforts focus only on systems supporting isolated EPs characterized by increased sensitivity to external perturbations, which makes them potential candidates for building next generation optical sensors. On the downside, this feature is also the Achilles heel of these devices: they are very sensitive to fabrication errors and experimental uncertainties. To overcome this problem, we introduce a new design concept for implementing photonic EPs that combine the robustness required for practical use together with their hallmark sensitivity. Particularly, our proposed structure exhibits a hypersurface of Jordan EPs (JEPs) embedded in a larger space, and having the following peculiar features: (1) A large class of undesired perturbations shift the operating point along the exceptional surface (ES), thus leaving the system at another EP which explains the robustness; (2) Perturbations due to back reflection/scattering force the operating point out of the ES, leading to enhanced sensitivity. Importantly, our proposed geometry is relatively easy to implement using standard photonics components and the design concept can be extended to other physical platforms such as microwave or acoustics.

Exceptional points (EP) are peculiar singularities that arise in non-Hermitian Hamiltonians when two or more eigenstates coalesce [1–6]. The resultant reduction in the eigenstate space dimensionality renders these points very sensitive to any external perturbations. Current research works in non-Hermitian and parity-time (PT) symmetric physics [7, 8] have so far focused on systems supporting isolated EPs in a reduced parameter space. This strategy has allowed researchers to investigate certain important aspects of non-Hermitian systems and gain insight into their behavior [9–24]. This however comes at a price: isolated EPs are very sensitive to unavoidable fabrication errors or experimental uncertainty (e.g. small variation in the experimental conditions). To better appreciate this point, consider the current implementations of photonic EPs based on PT-symmetric coupled elements [9–12] or engineered back reflection [25–28]. In both of these geometries, which have been recently exploited to demonstrate ultra-responsive optical sensors [28, 29], the design parameters have to be tailored precisely in order to force the system to operate at an EP. In the PT-symmetric implementation [29], the resonant frequencies of the two rings have to be identical; the gain/loss profiles have to be exactly balanced; and the difference between the gain and loss values has to match the coupling coefficient between the two resonators. Alternatively, in the single ring implementation [25–28], the sizes and locations of the nanoscatterers next to the ring have to be controlled with high precision during the fabrication. To overcome these difficulties, various research teams employ clever techniques (such as micro-heaters and movable fiber tips,

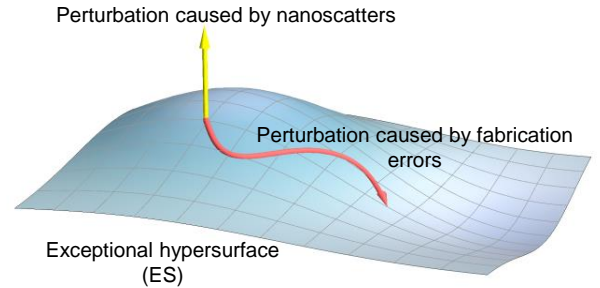


FIG. 1. A non-Hermitian photonic structure can combine robustness together with sensitivity if it exhibits a hypersurface of exceptional points with the following properties: (1) Undesired perturbations due to fabrication imperfections and experimental uncertainties shift the spectrum across the surface, leaving the system at an EP; (2) Perturbations accounting for the quantities to be measured force the spectrum out of the surface, i.e. away from EPs.

tunable coupling, etc) in order to actively and continuously tune the studied systems in the vicinity of the EPs. Beyond these important proof-of-concept demonstrations, it will be extremely useful for practical sensing applications to advance new design concepts that decouple the effects of fabrication errors and experimental uncertainties from perturbations caused by measurements.

In this letter, we present a new non-Hermitian photonic structure that exhibits an exceptional hypersurface (ES) embedded in a high-dimensional parameters space.

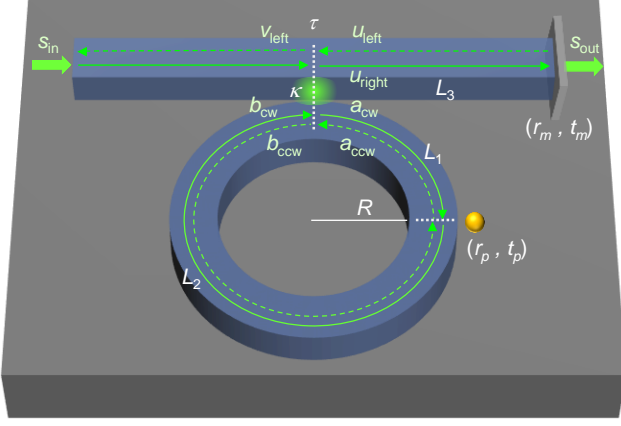


FIG. 2. Schematic diagram of the proposed photonic structure that satisfies the criteria mentioned in Fig. 1. It consists of a microring resonator coupled to a waveguide that has a mirror on one side and reflectionless at the other end. The relevant design parameters are indicated in the figure (see SM for details). In the absence of any reflective perturbations, the system exhibits an EP. Any variations of the coupling coefficients or the resonant frequency of the cavity will still leave the system at an EP. On the other hand, if a nanoscatterer (or any other form of reflective perturbations) comes to the vicinity of the ring, it will introduce a bidirectional coupling between the clockwise (CW) and counterclockwise (CCW) waves and shift the system away from the EP which in turn will leave a fingerprint on the emission spectrum of the system (if used in the lasing regime) or the power scattering spectrum (if operated in the amplification regime).

This, in turn, provides additional degrees of freedom that can be exploited to combine robustness with enhanced sensitivity. Particularly, robustness can be achieved if the system's response is tailored such that a large class of fabrication errors and experimental uncertainties shift the operating point along the ES. On the other hand, enhanced sensitivity can arise if the perturbation due to the measurements forces the spectrum away from the ES, causing large splitting of the resonant frequency (as compared to that associated with diabolic points (DP) [30–36]). This generic concept is illustrated schematically in Fig. 1. Here we show that this concept can be implemented by using standard photonic technology, which paves the way towards practical applications of non-Hermitian photonic sensors.

To this end, we consider the structure depicted schematically in Fig. 2. It consists of a single microring resonator coupled to a waveguide. One end of this waveguide is terminated by a mirror while the other end is assumed to be reflectionless (see Supplementary Material (SM) for the effect of finite small reflectivity [37]). Within the context of coupled mode theory, the above structure in the absence of the scatterer can be described

by the effective Hamiltonian:

$$i \frac{d}{dt} \begin{bmatrix} \tilde{a}_{cw} \\ \tilde{a}_{ccw} \end{bmatrix} = H_{ES} \begin{bmatrix} \tilde{a}_{cw} \\ \tilde{a}_{ccw} \end{bmatrix}, H_{ES} = \begin{bmatrix} \omega_0 - i\gamma & 0 \\ \alpha\mu^2 & \omega_0 - i\gamma \end{bmatrix} \quad (1)$$

where $\tilde{a}_{cw,ccw}$ are the field amplitudes of the clockwise (CW) and counterclockwise (CCW) modes, ω_0 is the resonant frequency, γ is the cavity loss rate which can be decomposed into intrinsic absorption, radiation loss, and loss to the waveguide (i.e. $\gamma = \gamma_{abs} + \gamma_{rad} + \mu^2/2$), and μ quantifies the coupling rate between the resonator and the waveguide. In addition, $\alpha = r_m \exp(i2\phi_3)$ where r_m is the field reflection coefficient at the mirror and $\phi_3 = \beta_w L_3$. Here β_w is the propagation constant of the waveguide and the distances L_3 are depicted in Fig. 2. Note that the above form of the Hamiltonian does not imply that the system is nonreciprocal, i.e. the transmission between the input and out ports is the same if the role of the two ports is reversed.

The eigenvalues of H_{ES} as written in the bases $\exp(-i\omega t)$, together with the associated eigenvectors $\tilde{\mathbf{a}}_{1,2}$ are given by:

$$\begin{aligned} \omega_{1,2} &= \omega_0 - i\gamma, \\ \tilde{\mathbf{a}}_{1,2} &= (0, 1)^T. \end{aligned} \quad (2)$$

The spectrum of the Hamiltonian H_{ES} features an EP with two identical eigenmodes characterized by a finite CCW component and a null CW component. Importantly, this is even true for any value of ω_0 , γ and $\alpha\mu^2$. In other words, there is hypersurface spanned by all possible values of these parameters where the system remains at an EP. For instance, if the fabricated system has extra (less) loss, stronger (weaker) coupling to the waveguide or a shift in its resonance frequency from the original targeted values, the system will be still located at an EP without the need for any external tuning. Only perturbations that introduce differential loss, frequency mismatch or additional coupling between the two modes (CW and CCW) can affect the system performance. However, these perturbations do not arise naturally in our proposed design since any change in the size of the resonator or its coupling to the waveguide will affect both modes symmetrically [43]. This unique feature provides unprecedented robustness that cannot be achieved in standard non-Hermitian systems that rely on isolated EPs in the design parameter space. However, in the presence of a nanoscatterer located in the vicinity of the ring resonator, the interaction between the scatterer and the evanescent field of the optical modes introduces a bidirectional coupling between the CW and CCW modes, which are described by additional corrections of the same order to both off-diagonal matrix elements of H_{ES} , say ϵ . If we further assume that ϵ is much smaller than other matrix elements, it is straightforward to show that the splitting of the eigenfrequency is $\Delta\omega \equiv |\omega_1 - \omega_2| \sim \sqrt{\epsilon}$. In standard waveguide-coupled microring resonators operating

at a diabolic point, this splitting will be rather ϵ . Thus, in addition to its robustness, the proposed system is expected to also provide enhanced sensitivity.

In order to put this discussion on a more solid ground while at the same time elucidate on the relevant experimental parameters, we study the above structure using the scattering matrix method (SMM) [49–51]. Here we assume that the system is probed via the waveguide by a signal s_{in} . We then proceed to calculate the output signal s_{out} as a function of the input frequency for different levels of perturbation by a nanoscatterer, which we quantify by its location as well as reflection/transmission coefficients r_p/t_p , respectively (see Fig. 2 and SM for a full list of parameters).

By doing so, we obtain (see SM for scattering matrix method):

$$\frac{s_{\text{out}}}{s_{\text{in}}} = \frac{e^{i\phi_3} t_m [(1 + e^{2i\phi})\tau - e^{i\phi}(1 + \tau^2)t_p]}{1 + e^{i2\phi}\tau^2 - 2e^{i\phi}\tau t_p - e^{2i\phi'} r_m r_p \kappa^2} \equiv \frac{N}{D}, \quad (3)$$

where $\phi = \phi_1 + \phi_2$ and $\phi' = \phi_2 + \phi_3$, with $\phi_{1,2} = \beta_r L_{1,2}$ and $\phi_3 = \beta_w L_3$. In general, the values of propagation constants associated with the ring and straight waveguides, $\beta_{r,w}$, can be complex with the imaginary parts accounting for the possible radiation and material loss as well as the gain (loss due to coupling to the waveguide is treated separately). For reasons that will be clear shortly, we are particularly interested in the case of active devices where the microring exhibits enough optical gain to bring the system at or close to the lasing condition (for completeness we treat the passive case in SM [52]). Under either of these conditions, the lasing or the transmission spectrum (respectively) is dominated by the the poles of the power scattering coefficient $T = |s_{\text{out}}/s_{\text{in}}|^2$, or equivalently the zeros of D . To characterize the performance of the proposed structure, we thus study the behavior of D as a function of the particle reflectivity r_p and the input frequency parametrized by ϕ (we do not take the waveguide dispersion into account at this moment), i.e. $D \equiv D(r_p, \phi)$.

For any set of design parameters and a specific value of r_p , the lasing conditions is achieved for values of $\phi \equiv \phi_D$ satisfying the equation $D(r_p, \phi_D) = 0$, which gives $\exp(i\phi_D^\pm) = \tau^{-1}(t_p \pm i\sqrt{r_p^2 - \exp(2i\phi')r_m \kappa^2 r_p})$. The maximum frequency splitting $\Delta\phi \equiv \text{Re}[\phi_D^+ - \phi_D^-]$ occurs when $\exp[2i\text{Re}(\phi')] = -1$. As a side comment, we note that $\text{Im}[\phi_D] = -\kappa^2/2$, which implies the lasing threshold occurs when the gain is enough to compensate for the radiation/material loss as well as the loss due to coupling to the waveguide, as one would expect. By writing $r'_m = r_m \times |\exp(2i\phi')|$ we find:

$$\Delta\phi = 2\sqrt{r_p^2 + r'_m \kappa^2 r_p}. \quad (4)$$

In Eq. (4), $r'_m \kappa^2$ is the effective unidirectional coupling from CW mode to CCW mode. By noting that in our

systems, both r_m and $|\exp(2i\phi')| = \exp(-2\text{Im}[\phi'])$ are in the order of unity (since the system is assumed to operate below but close to the lasing threshold), we arrive at:

$$\Delta\phi_{\text{EP}} \approx \begin{cases} 2\kappa\sqrt{r_p}, & r_p \ll \kappa^2 \\ 2r_p, & r_p \gg \kappa^2 \end{cases}, \quad (5)$$

$$\Delta\phi_{\text{DP}} = 2r_p. \quad (6)$$

Equation (5) is the central result of this work. It confirms the existence of an operating regime ($r_p \ll \kappa^2$) where the frequency splitting scales with the square root function of the perturbation, which is the hallmark of enhanced sensitivity near a second-order EP. Beyond this regime, the splitting is linear as in standard sensors operating at a diabolic point. Intuitively, as the perturbation due to the scatterer shifts the system far away from the EP, the extra sensitivity is lost. In comparison, as shown by Eq. (6), which describes the same non-Hermitian system in the absence of the mirror (i.e. operating at a DP), the splitting is linear from the very beginning.

In the active scattering regime, when the gain brings the system relatively close to the lasing point but remains below the lasing threshold, the transmission peaks can be obtained by solving Eq. (3). Not surprisingly, here also the locations of the transmission peaks are dominated by the zeros of $D(r_p, \phi)$, which again results in a square-root dependence of the frequency splitting as we have confirmed numerically.

Having discussed the essential features of the proposed structure, we now confirm our predictions by performing two-dimensional(2D) full-wave Finite-Difference Time-Domain (FDTD) simulations [55] using realistic material platforms. Particularly, we study a 2D version of the schematic shown in Fig. 2. It consists of a microring resonator having a refractive index $n_2 = 1.45$, a radius $R = 10 \mu\text{m}$, and a width $w = 0.8 \mu\text{m}$. The ring is coupled to a waveguide having the same material and width. The edge-to-edge separation between the ring and the waveguide is chosen to be $d = 0.6 \mu\text{m}$, corresponding to $\kappa^2 = 0.028$. A mirror with reflectivity $r_m = 0.99$ is introduced at one end of the waveguide via a 50-nm-thick silver layer. To simulate the perturbation induced by a nanoscatterer, we use a disk assumed to be of the same material with the waveguide and vary its radius in the simulation from 20 nm to 100 nm. The disk is located at 3 o'clock with a fixed distance $h = 0.1 \mu\text{m}$ from its center to the outside of the microring. Based on the chosen position of the nanoscatterer, we set $L_3 = 10.075 \mu\text{m}$, which results in an optimal operation (defined by the maximum frequency splitting and peak visibility) for a test particle having a 30 nm radius. Finally, the background material is assumed to be air of $n_1 = 1$. In our simulations, the device is probed by a TE-polarized broad bandwidth pulse with central frequency at $f = 193.4 \text{ THz}$ or equivalently $\lambda = 1550 \text{ nm}$ (almost matching one of the longitudinal modes of the microring) launched from the left side of

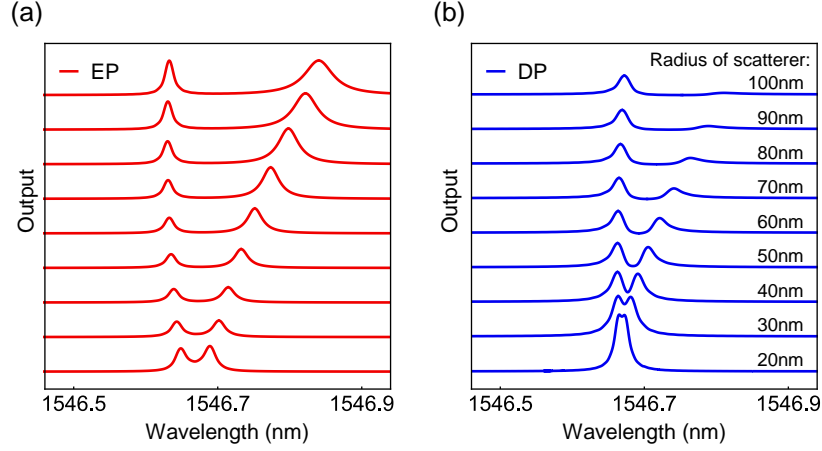


FIG. 3. Finite difference time domain simulations for a system similar to that of Fig. 2. (a) and (b) plot the spectrum splitting as a function of nanoscatterer size. Clearly, the EP-based structure demonstrates superior performance in terms of the splitting magnitude and the visibility of the resonance peaks.

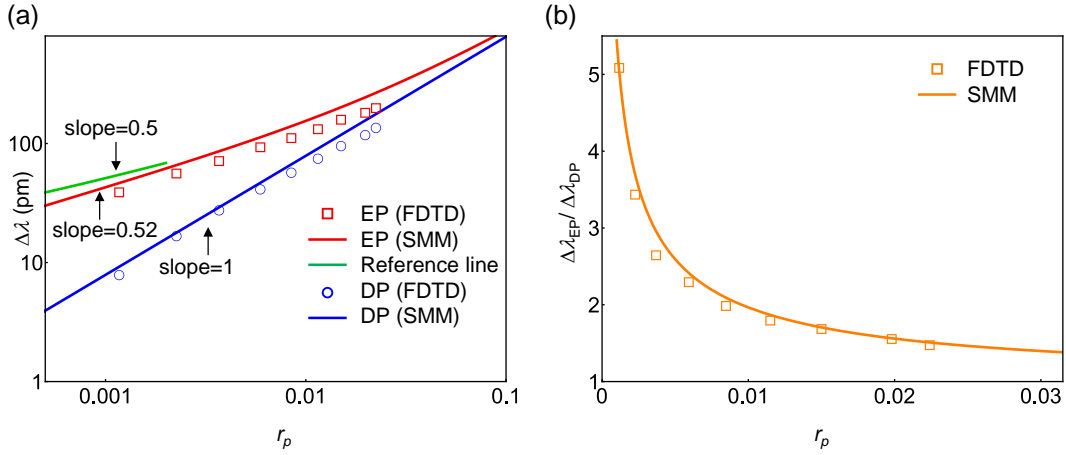


FIG. 4. Sensitivity enhancement as a function of the nanoscatterer radius. Clearly the EP sensor has a better performance than a sensor operating at a DP for smaller scatterer, making this device valuable for measuring small perturbations. In producing the solid lines, we first used FDTD simulations to simulate subsystems of the full structure to extract the design parameters (for example, using the waveguide and mirror only without the resonator to compute the mirror reflectivity; or the ring resonator only and the scatterer to compute the scatterer reflectivity, etc). Next, we used these extracted parameters in our analytical formulas (4-6) together with the definition of ϕ in order to produce the solid lines.

the waveguide. In order to isolate the relevant transmission peaks in our simulations, we used a dispersive gain function as described in SM.

Figures 3(a) and (b) show the transmission spectrum for the cases of EP and DP, respectively for the parameters listed in the figure caption. Evidently, the EP-based device exhibits a significant advantage, demonstrating larger splitting and clear transmission peaks. Note that the location of one transmission peak remains almost invariant while the other experience red-shift. This can be explained by the scatterer-induced coupling between different wave components [34, 56]. A more quantitative explanation based on perturbation theory is also pro-

vided in the SM [57]. Figure 4(a) plots a log-log scale of the slopes characterizing the magnitude of the splitting, where the superior performance of EP is evident. This conclusion is better illustrated in Fig. 4(b), which depicts the enhancement factor (defined as the ratio of the splitting in the EP case normalized by that of the DP case) of the proposed sensor as a function of the nanoscatterer reflectivity r_p when the scatterer size is varied from 20 nm to 100 nm [59]. These figures also demonstrate the excellent agreement between the FDTD (square points) and the scattering matrix method (solid lines).

In conclusion, we have proposed a new class of non-Hermitian sensors that operate at exceptional surfaces

as opposed to isolated exceptional points. This new paradigm provides more degrees of freedom that can be exploited to combine a certain degree of robustness against fabrication tolerance (which is crucial for real-life applications) together with the enhanced sensitivity associated with exceptional points. We also expect our proposed system to demonstrate some robustness against the type of thermal fluctuations studied recently in [61] (see SM [62]). Interestingly, it was recently shown that non-Hermitian Hamiltonians with unidirectional coupling (i.e. similar to that used in our proposed work) can exhibit superior performance even in the quantum regime [64]. We anticipate that our results, together with recent work on exceptional surface in photonic crystals [65], will open a host of new possibilities for sensing applications using practical non-Hermitian devices. Importantly, the proposed design concept presented here can be implemented in other physical platforms such as acoustics or microwaves.

* Corresponding author: ganainy@mtu.edu

- [1] W. D. Heiss and A. L. Sannino, *J. Phys. A* **23**, 1167 (1990).
- [2] A. I. Magunov, I. Rotter, and S. I. Strakhova, *J. Phys. B* **32**, 1669 (1999).
- [3] W. D. Heiss, *J. Phys. A* **37**, 2455 (2004).
- [4] W. D. Heiss, *J. Phys. A* **45**, 444016 (2012).
- [5] I. Rotter, *Phys. Rev. E* **67**, 026204 (2003).
- [6] M. Müller and I. Rotter, *J. Phys. A* **41**, 244018 (2008).
- [7] R. El-Ganainy, K. G. Makris, M. Khajavikhan, Z. H. Musslimani, S. Rotter, and D. N. Christodoulides, *Nat. Phys.* **14**, 11 (2018).
- [8] L. Feng, R. El-Ganainy, and L. Ge, *Nat. Photon.* **11**, 752 (2017).
- [9] C. E. Rüter, K. G. Makris, R. El-Ganainy, D. N. Christodoulides, M. Segev, and D. Kip, *Nat. Phys.* **6**, 192 (2010).
- [10] B. Peng, Ş. K. Özdemir, F. Lei, F. Monifi, M. Gianfreda, G. L. Long, S. Fan, F. Nori, C. M. Bender, and L. Yang, *Nat. Phys.* **10**, 394 (2014).
- [11] M. Brandstetter, M. Liertzer, C. Deutsch, P. Klang, J. Schöberl, H. E. Türeci, G. Strasser, K. Unterrainer, and S. Rotter, *Nat. Commun.* **5**, 4034 (2014).
- [12] H. Hodaei, M.-A. Miri, M. Heinrich, D. N. Christodoulides, and M. Khajavikhan, *Science* **346**, 975 (2014).
- [13] J. Schindler, A. Li, M. C. Zheng, F. M. Ellis, and T. Kottos, *Phys. Rev. A* **84**, 040101(R) (2011).
- [14] Z. Lin, H. Ramezani, T. Eichelkraut, T. Kottos, H. Cao, and D. N. Christodoulides, *Phys. Rev. Lett.* **106**, 213901 (2011).
- [15] M. Liertzer, L. Ge, A. Cerjan, A. D. Stone, H. E. Türeci, and S. Rotter, *Phys. Rev. Lett.* **108**, 173901 (2012).
- [16] Q. Zhong, D. N. Christodoulides, M. Khajavikhan, K. G. Makris, and R. El-Ganainy, *Phys. Rev. A* **97**, 020105(R) (2018).
- [17] P. Ambichl, K. G. Makris, L. Ge, Y. Chong, A. D. Stone, and S. Rotter, *Phys. Rev. X* **3**, 041030 (2013).
- [18] G. Castaldi, S. Savoia, V. Galdi, A. Alù, and N. Engheta, *Phys. Rev. Lett.* **110**, 173901 (2013).
- [19] E. Rivet, A. Brandstetter, K. G. Makris, H. Lissek, S. Rotter, and R. Fleury, *Nat. Phys.* **14**, 942 (2018).
- [20] J. Zhang, B. Peng, Ş. K. Özdemir, K. Pichler, D. O. Krimer, G. Zhao, F. Nori, Y.-x. Liu, S. Rotter, and L. Yang, *Nat. Photon.* **12**, 479 (2018).
- [21] L. Feng, Y.-L. Xu, W. S. Fegadolli, M.-H. Lu, J. E. B. Oliveira, V. R. Almeida, Y.-F. Chen, and A. Scherer, *Nat. Mater.* **12**, 108 (2012).
- [22] L. Feng, Z. J. Wong, R.-M. Ma, Y. Wang, and X. Zhang, *Science* **346**, 972 (2014).
- [23] S. Longhi, *Phys. Rev. Lett.* **103**, 123601 (2009).
- [24] P.-Y. Chen, M. Sakhdari, M. Hajizadegan, Q. Cui, M. M.-C. Cheng, R. El-Ganainy, and A. Alù, *Nat. Electron.* **1**, 297 (2018).
- [25] J. Wiersig, *Phys. Rev. A* **84**, 063828 (2011).
- [26] J. Wiersig, *Phys. Rev. Lett.* **112**, 203901 (2014).
- [27] J. Wiersig, *Phys. Rev. A* **93**, 033809 (2016).
- [28] W. Chen, Ş. K. Özdemir, G. Zhao, J. Wiersig, and L. Yang, *Nature* **548**, 192 (2017).
- [29] H. Hodaei, A. U. Hassan, S. Wittek, H. Garcia-Gracia, R. El-Ganainy, D. N. Christodoulides, and M. Khajavikhan, *Nature* **548**, 187 (2017).
- [30] T. J. Kippenberg, S. M. Spillane, and K. J. Vahala, *Opt. Lett.* **27**, 1669 (2002).
- [31] T. J. Kippenberg, A. L. Tchebotareva, J. Kalkman, A. Polman, and K. J. Vahala, *Phys. Rev. Lett.* **103**, 027406 (2009).
- [32] L. He, Ş. K. Özdemir, J. Zhu, and L. Yang, *Phys. Rev. A* **82**, 053810 (2010).
- [33] W. Kim, Ş. K. Özdemir, J. Zhu, F. Monifi, C. Coban, and L. Yang, *Opt. Express* **20**, 29426 (2012).
- [34] J. Zhu, Ş. K. Özdemir, Y.-F. Xiao, L. Li, L. He, D.-R. Chen, and L. Yang, *Nat. Photon.* **4**, 46 (2010).
- [35] Ş. K. Özdemir, J. Zhu, X. Yang, B. Peng, H. Yilmaz, L. He, F. Monifi, S. H. Huang, G. L. Long, and L. Yang, *Proc. Natl. Acad. Sci. U.S.A.* **111**, E3836 (2014).
- [36] M. R. Foreman, J. D. Swaim, and F. Vollmer, *Adv. Opt. Photonics* **7**, 168 (2015).
- [37] See SM at <http://link.aps.org/supplemental/xxx> for eliminating refection from input port, which includes Refs. [38–42].
- [38] M. Mundbrod, Annual Report 2003, Optoelectronics Department, University of Ulm (2003).
- [39] Q. Chen, X. Zhou, Y. Wang, Q. Huang, X. Chen, and W. Jiang, in *International Conference on Optical Instruments and Technology 2017*, Vol. 10622 (SPIE, 2017) p. 8.
- [40] I. Kaminow, G. Eisenstein, and L. Stulz, *IEEE J. Quantum Electron.* **19**, 493 (1983).
- [41] B. J. H. Stadler and T. Mizumoto, *IEEE Photonics Journal* **6**, 1 (2014).
- [42] D. Ye, C. Cao, T. Zhou, J. Huangfu, G. Zheng, and L. Ran, *Nat. Commun.* **8**, 51 (2017).
- [43] See SM at <http://link.aps.org/supplemental/xxx> for effect of surface roughness and resonator's shape, which includes Refs. [44–48].
- [44] B. E. Little, J.-P. Laine, and S. T. Chu, *Opt. Lett.* **22**, 4 (1997).
- [45] J. Wiersig, S. W. Kim, and M. Hentschel, *Phys. Rev. A* **78**, 053809 (2008).
- [46] A. J. Maker and A. M. Armani, *J. Vis. Exp.*, e4164 (2012).

- [47] M. M. Lee, J. Yao, and M. C. Wu, in *18th IEEE International Conference on Micro Electro Mechanical Systems, 2005. MEMS 2005.*, pp. 596–599.
- [48] X. Ji, F. A. S. Barbosa, S. P. Roberts, A. Dutt, J. Cardenas, Y. Okawachi, A. Bryant, A. L. Gaeta, and M. Lipson, *Optica* **4**, 619 (2017).
- [49] A. Yariv, *Electron. Lett.* **36**, 321 (2000).
- [50] V. Van, *Optical Microring Resonators: Theory, Techniques, and Applications*, 1st ed. (CRC Press, Boca Raton, Florida, 2017).
- [51] B. E. A. Saleh and M. C. Teich, *Fundamentals of Photonics*, 2nd ed. (Wiley, Hoboken, New Jersey, 2007).
- [52] See SM at <http://link.aps.org/supplemental/xxx> for passive EP sensors, which includes Refs. [53, 54].
- [53] T. J. Kippenberg, *Nat. Photon.* **4**, 9 (2010).
- [54] A. Yariv, *IEEE Photonics Technol. Lett.* **14**, 483 (2002).
- [55] A. Taflov and S. C. Hagness, *Computational Electrodynamics: The Finite-Difference Time-Domain Method*, 3rd ed. (Artech House, Boston, London, 2005).
- [56] J. Zhu, S. K. Ozdemir, L. He, and L. Yang, *Opt. Express* **18**, 23535 (2010).
- [57] See SM at <http://link.aps.org/supplemental/xxx> for asymmetric shift in the transmission peaks, which includes Ref. [58].
- [58] S. G. Johnson, M. Ibanescu, M. A. Skorobogatiy, O. Weisberg, J. D. Joannopoulos, and Y. Fink, *Phys. Rev. E* **65**, 066611 (2002).
- [59] See SM at <http://link.aps.org/supplemental/xxx> for reflection from nanoscatterer, which includes Ref. [60].
- [60] J. Zhu, Y. Zhong, and H. Liu, *Photon. Res.* **5**, 396 (2017).
- [61] C. Wolff, C. Tserkezis, and N. A. Mortensen, [arXiv:1810.08390](https://arxiv.org/abs/1810.08390) (2018).
- [62] See SM at <http://link.aps.org/supplemental/xxx> for temperature sensitivity, which includes Ref. [63].
- [63] T. Toyoda and M. Yabe, *J. Phys. D* **16**, L97 (1983).
- [64] H.-K. Lau and A. A. Clerk, *Nat. Commun.* **9**, 4320 (2018).
- [65] H. Zhou, J. Y. Lee, S. Liu, and B. Zhen, *Optica* **6**, 190 (2019).